Supplement of Earth Syst. Dynam., 14, 345–365, 2023
https://doi.org/10.5194/esd-14-345-2023-supplement

Earth System Dynamics
Open Access
EGU

Supplement of

The implications of maintaining Earth's hemispheric albedo symmetry for shortwave radiative feedbacks

Aiden R. Jönsson and Frida A.-M. Bender

Correspondence to: Aiden R. Jönsson (aiden.jonsson@misu.su.se)

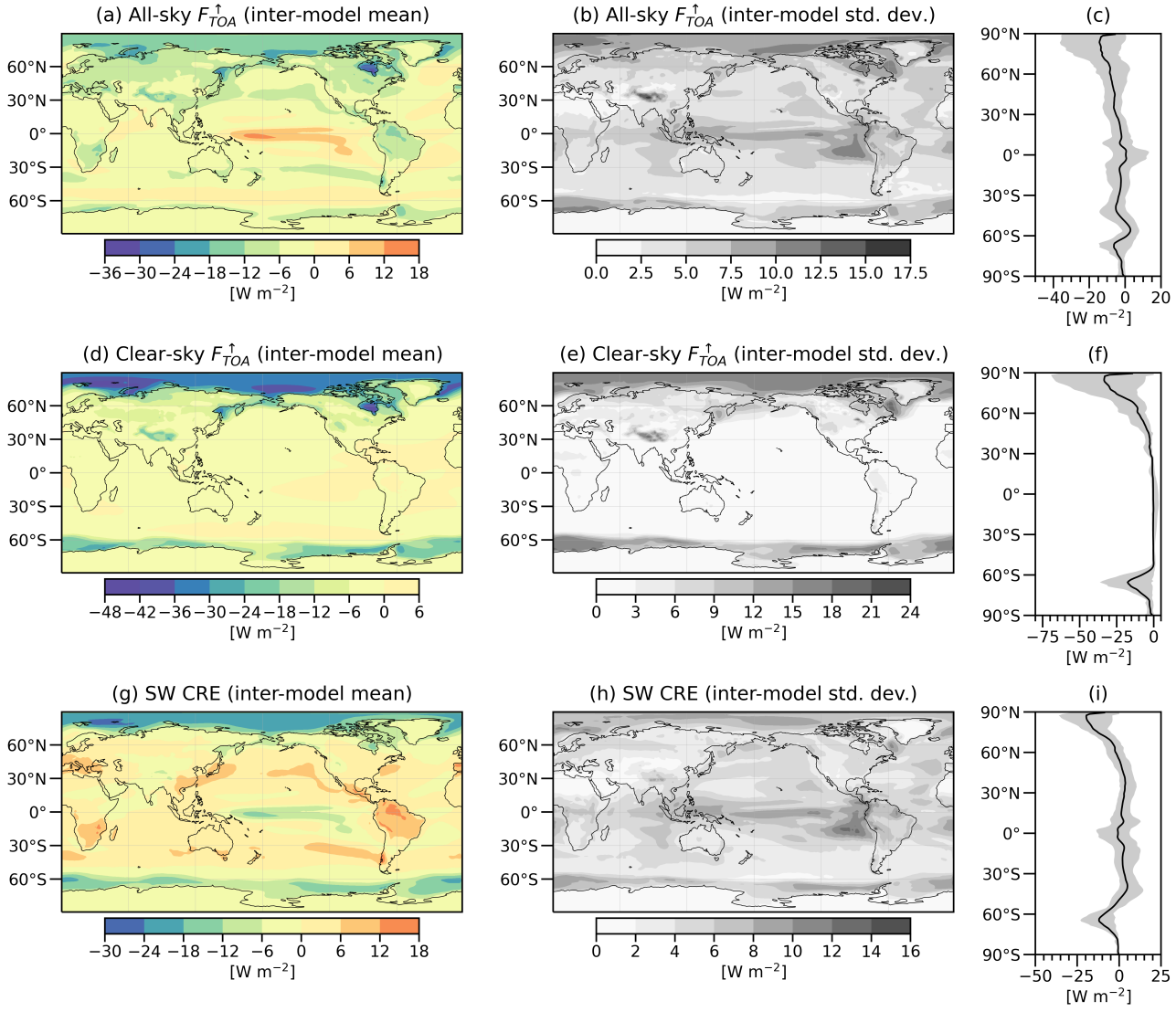

Supplementary Figure S1. Left column: inter-model mean differences in (a) all-sky and (d) clear-sky $F_{TOA}^{\uparrow}$, as well as (g) SW CRE, between 'Mid' and PI conditions. Middle column: standard deviation among models in differences between 'Mid' and PI conditions for (b) all-sky and (e) clear-sky $F_{TOA}^{\uparrow}$, as well as (h) SW CRE. Right column: inter-model mean profiles of zonal mean differences between 'Mid' and PI conditions in (a) all-sky and (d) clear-sky $F_{TOA}^{\uparrow}$, as well as (g) SW CRE; the gray shading represents model spread (minima and maxima of mean changes at each latitude).

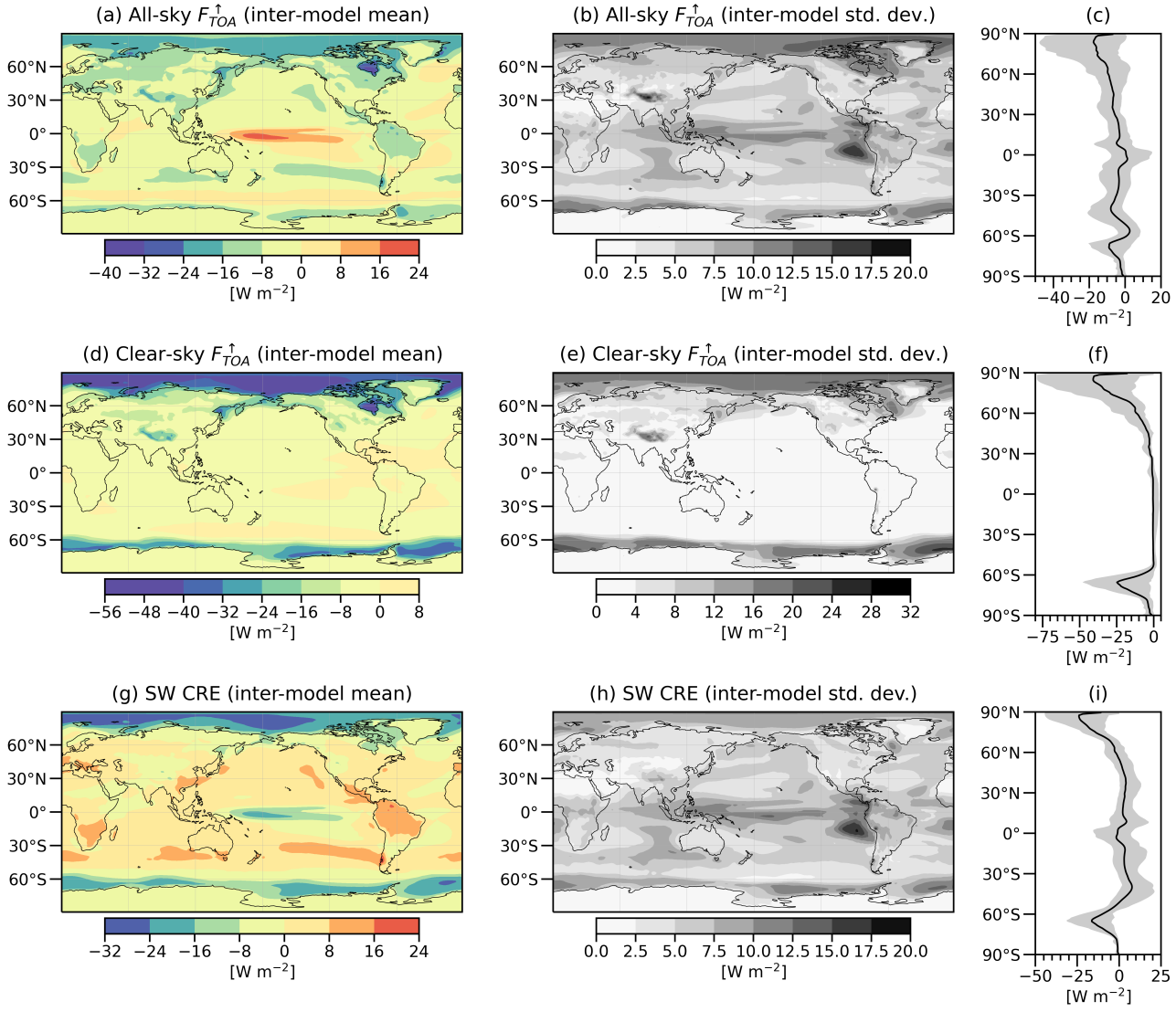

Supplementary Figure S2. Left column: inter-model mean differences in (a) all-sky and (d) clear-sky $F^{\uparrow}_{TOA}$, as well as (g) SW CRE, between 'Mid' and PI conditions. Middle column: standard deviation among models in differences between 'End' and PI conditions for (b) all-sky and (e) clear-sky $F^{\uparrow}_{TOA}$, as well as (h) SW CRE. Right column: inter-model mean profiles of zonal mean differences between 'End' and PI conditions in (a) all-sky and (d) clear-sky $F^{\uparrow}_{TOA}$, as well as (g) SW CRE; the gray shading represents model spread (minima and maxima of mean changes at each latitude).

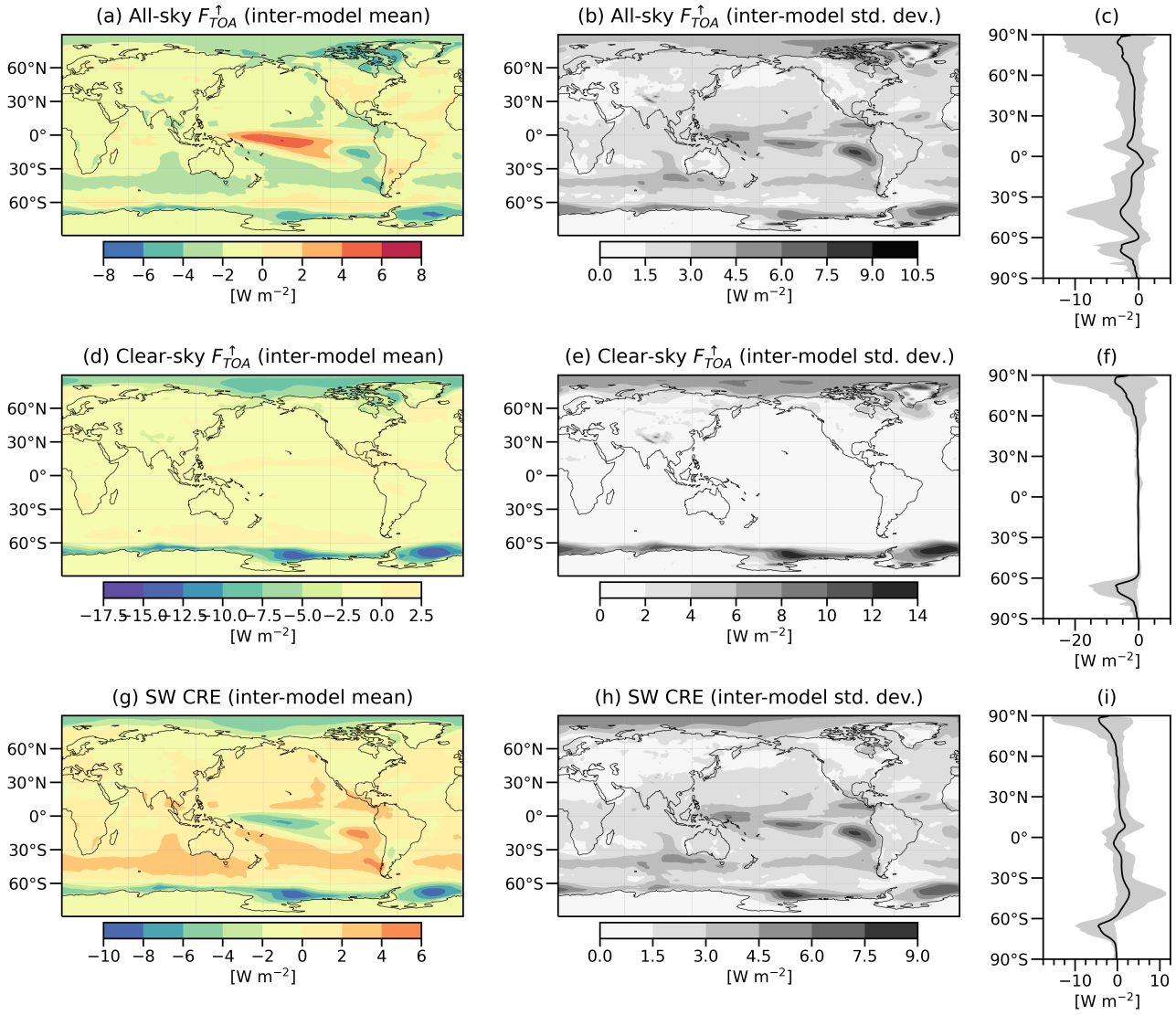

Supplementary Figure S3. Left column: inter-model mean differences in (a) all-sky and (d) clear-sky $F_{TOA}^{\uparrow}$, as well as (g) SW CRE, between 'Mid' and PI conditions. Middle column: standard deviation among models in differences between the 'End' and 'Mid' periods for (b) all-sky and (e) clear-sky $F_{TOA}^{\uparrow}$, as well as (h) SW CRE. Right column: inter-model mean profiles of zonal mean differences between the 'End' and 'Mid' periods in (a) all-sky and (d) clear-sky $F_{TOA}^{\uparrow}$, as well as (g) SW CRE; the gray shading represents model spread (minima and maxima of mean changes at each latitude).

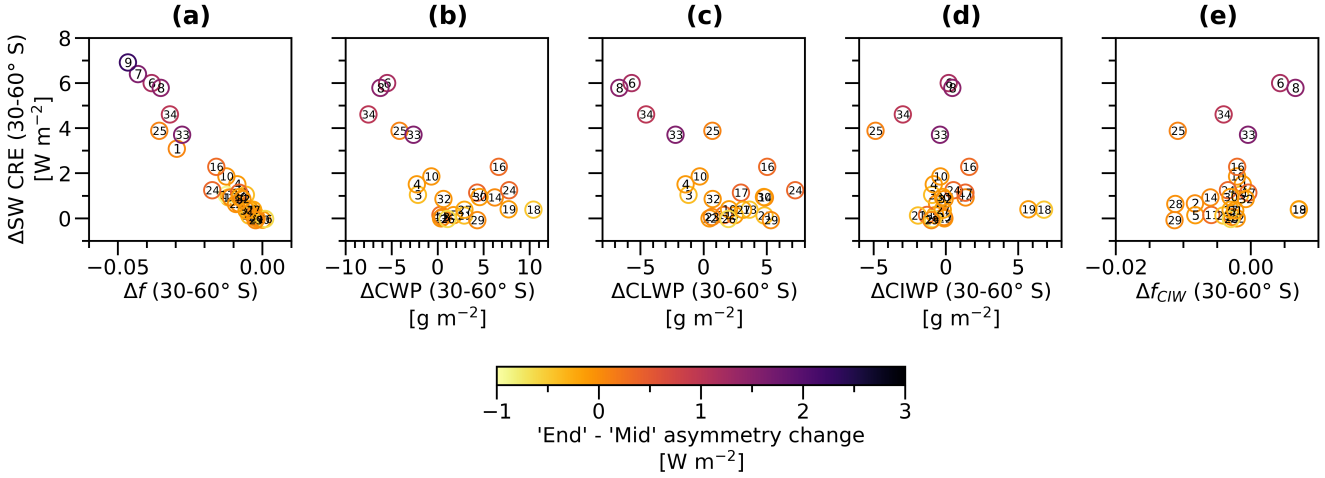

Supplementary Figure S4. Scatter plots showing 'End'-'Mid' differences in 30-60° S area mean (a) cloud fraction f, (b) in-cloud total water path CWP, (c) in-cloud liquid water path CLWP, (d) in-cloud ice water path CIWP, and (e) fraction of in-cloud ice to total water path f_{CIW} plotted against corresponding area mean 'End'-'Mid' differences in SW CRE. Markers denote models as they are numbered in Table 1. The color scale depicts changes in model asymmetry between 'End' and 'Mid'.

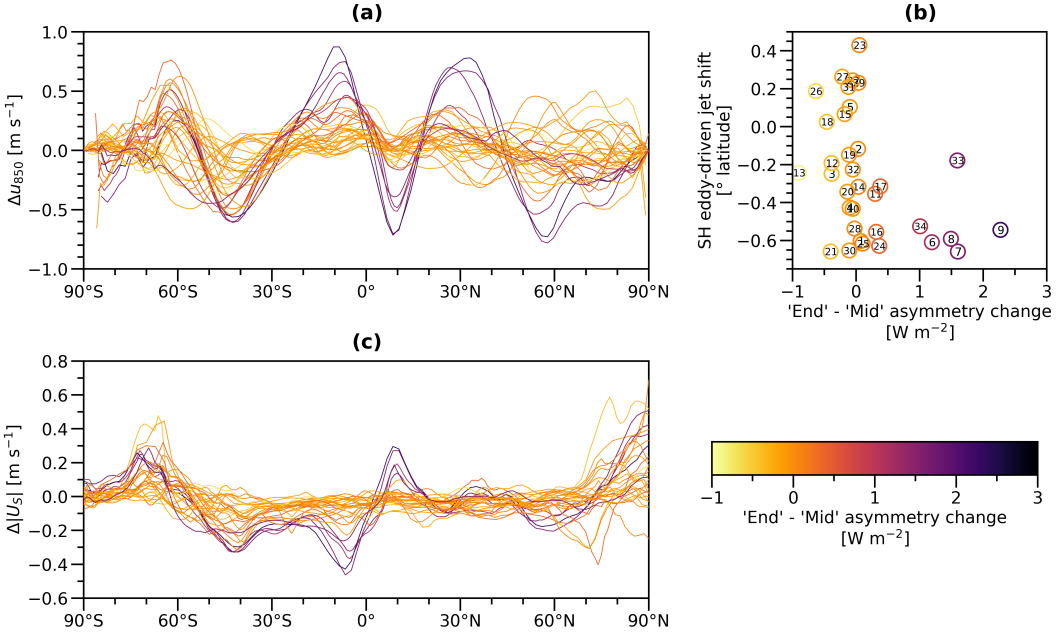

Supplementary Figure S5. (a) Meridional profile of differences in zonal mean zonal wind u at 850 hPa (u_{850}) between the 'End' and 'Mid' periods. (b) Mean difference of SH eddy-driven jet position between the 'End' and 'Mid' periods, plotted against the 'End' minus 'Mid' difference in area mean SW CRE over 30-60° S; the latitudinal positions of maxima of zonal mean u_{850} are here estimated by taking the meridional derivative of u_{850} and interpolating the intercept. The models are numbered as given in Table 1. (c) Meridional profile of differences in zonal mean near-surface wind speed $|U_S|$ between the 'End' and 'Mid' periods. The color scale represents the 'End' minus 'Mid' difference in asymmetry. Markers denote models as they are numbered in Table 1.

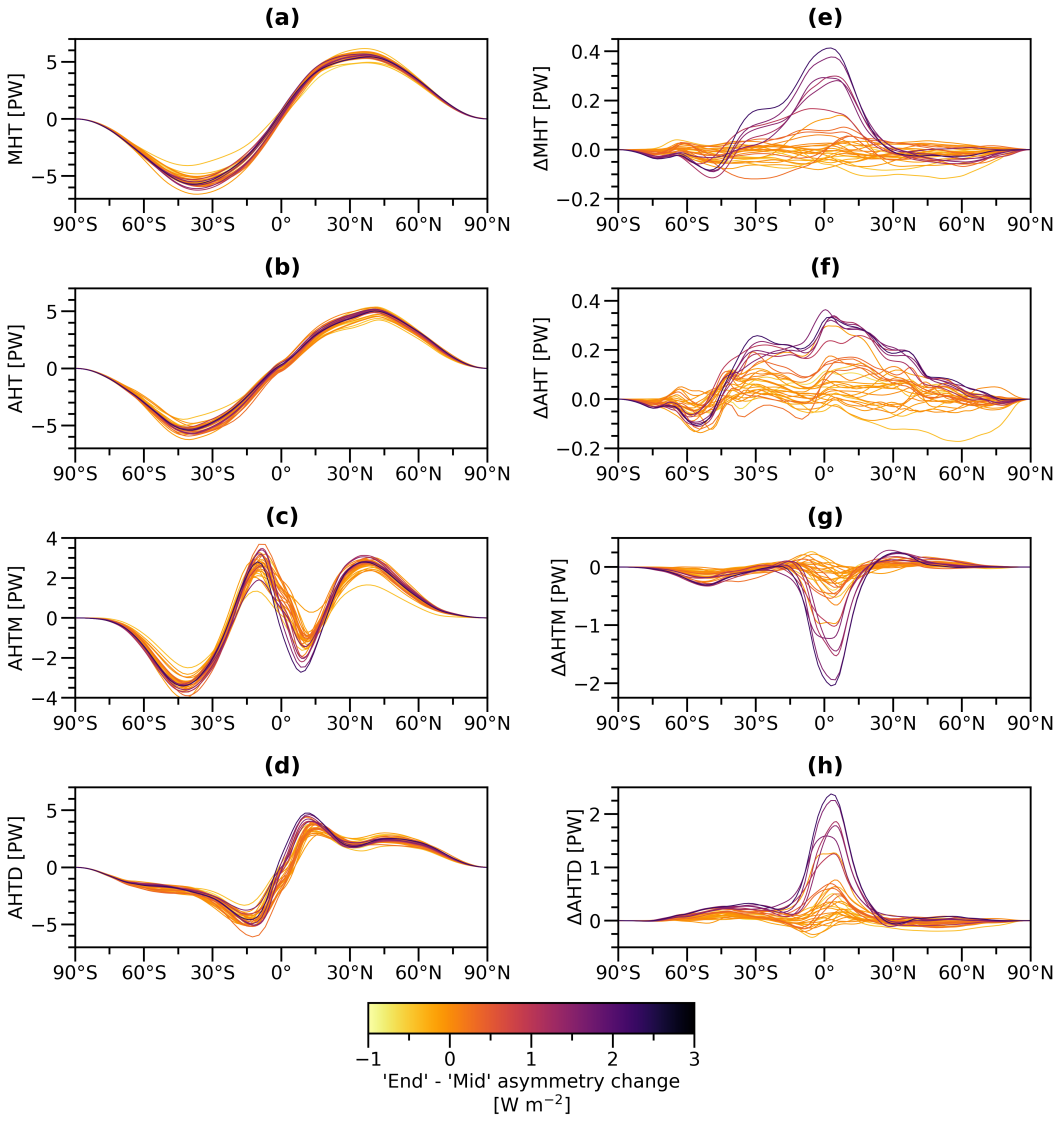

Supplementary Figure S6. Left column (a-d): mean profiles of inferred meridional heat transport (MHT) and its components (AHT: atmospheric heat transport; AHTM: moist atmospheric heat transport; and AHTD: dry atmospheric heat transport), respectively, as calculated in the method outlined in Section 2.2 during the 'End' period of the simulation (years 130-150). Right column (e-h): mean differences in MHT and its components AHT, AHTM, and AHTD, respectively, between the 'End' and 'Mid' periods. The color scale represents the 'End' minus 'Mid' difference in asymmetry.

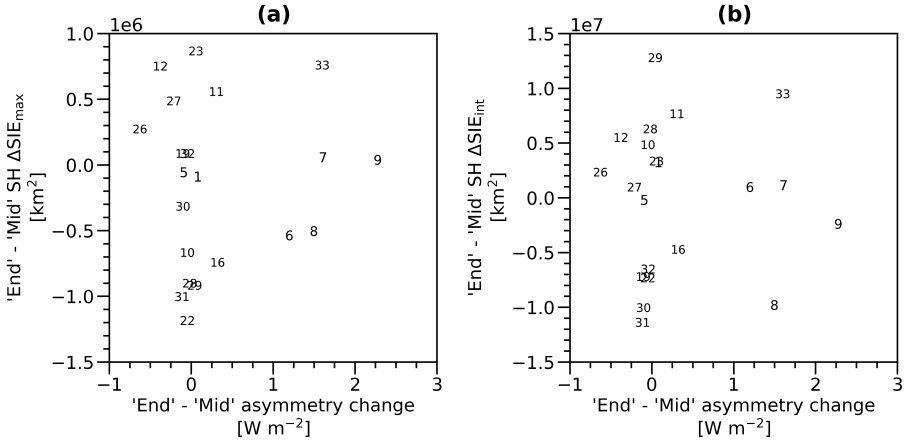

Supplementary Figure S7. Differences in 30-60° S mean SW CRE versus differences in (a) mean SH sea ice extent maxima $\mathrm{SIE}_{\mathrm{max}}$ (calculated by taking the annual maxima over seasonal cycles and then averaging over multiple years) and (b) annually integrated SH sea ice extent $\mathrm{SIE}_{\mathrm{int}}$ (calculated by taking annual sums of sea ice extent over annual cycles and then averaging over multiple years) between the 'End' and 'Mid' periods; the models are numbered as given in Table 1.